
SELF: A ROBUST SINGULAR VALUE AND EIGENVALUE APPROACH FOR LLM FINGERPRINTING

Hanxiu Zhang, Yue Zheng*

The Chinese University of Hong Kong, Shenzhen
 hanxiuzhang@link.cuhk.edu.cn, zhengyue@cuhk.edu.cn

ABSTRACT

The protection of Intellectual Property (IP) in Large Language Models (LLMs) represents a critical challenge in contemporary AI research. While fingerprinting techniques have emerged as a fundamental mechanism for detecting unauthorized model usage, existing methods—whether behavior-based or structural—suffer from vulnerabilities such as false claim attacks or susceptible to weight manipulations. To overcome these limitations, we propose SELF, a novel intrinsic weight-based fingerprinting scheme that eliminates dependency on input and inherently resists false claims. SELF achieves robust IP protection through two key innovations: 1) unique, scalable and transformation-invariant fingerprint extraction via singular value and eigenvalue decomposition of LLM attention weights, and 2) effective neural network-based fingerprint similarity comparison based on few-shot learning and data augmentation. Experimental results demonstrate SELF maintains high IP infringement detection accuracy while showing strong robustness against various downstream modifications, including quantization, pruning, and fine-tuning attacks. Our code is available at github.com/HanxiuZhang/SELF_v2.

Keywords Large Language Model · Intellectual Property Protection · Fingerprinting · Singular Values · Eigenvalues

1 Introduction

Large language models (LLMs) are increasingly being adopted as versatile tools to enhance productivity in various fields, including medical assistance ([1]), code generation ([2]), and so on. Developing a functional LLM requires substantial investments, including high-quality datasets, significant computational resources, and specialized human expertise. Consequently, protecting the intellectual property (IP) of LLMs is of paramount importance ([3]), particularly in the current era where open-source trends clash with the need for model creators to maintain naming conventions for attribution on derivative works.

Current model IP infringement detection methods primarily fall into two categories: watermarking and fingerprinting. Watermarking approaches embed identifiable features (watermarks) invasively into target models while trying to preserve their original functionality ([4, 5]). In contrast, fingerprinting methods extract unique model identifiers without modifying the model, either by analyzing the model’s input-output behavioral patterns ([6]) (i.e., behavior fingerprinting) or structural information (i.e., structural fingerprinting) such as weight distributions ([7]), intermediate representations ([8]), or gradient profiles ([9]). Compared to watermarking-based methods, fingerprinting schemes eliminate the need of retraining and avoid potential performance degradation associated with watermark insertion ([10]).

Despite these advantages, existing fingerprinting methods face critical limitations. Behavior-based techniques are vulnerable to false claim attacks ([11]), wherein malicious actors can falsely claim the ownership of independently trained models by crafting (transferable) adversarial samples. Although [12] propose to mitigate the attack by constructing fingerprints using targeted adversarial examples, the risk persists as such adversarial examples can still be transferrable albeit with greater difficulty. Structural approaches analyze model internal parameters but lack robustness against weight manipulations such as permutation or linear mapping. For schemes like HuRef ([7]) where the input is required to actively participate in fingerprint computation, we further extend the scope of false claim attack as malicious accuser can manipulate ownership verification results through carefully crafted input. Under this broader definition, we

*Corresponding author

conducted false claim attack on HuRef scheme and successfully manipulated the similarity score output (see Appendix B).

To address these issues, we propose a structural fingerprinting method named SELF, which purely depends on the model weights. Figure 1 describes SELF’s pipeline. The owner first extracts a fingerprint from the target model and trains a Similarity Network (*SimNet*) for verification. If the model is stolen, the owner can detect piracy by *SimNet*’s high similarity output. SELF comprises two key components: (1) *Fingerprint Extraction*, which derives unique, robust and scalable fingerprints from model weights; and (2) *Similarity Computation*, where a neural network learns fingerprint patterns to enable robust and efficient similarity assessment.

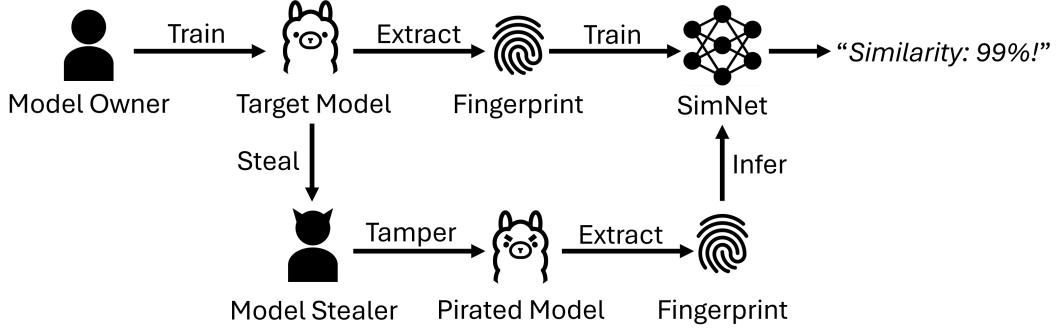


Figure 1: IP infringement detection pipeline using SELF.

In the fingerprint extraction module, we address potential model weight tampering caused by transformation attacks (e.g., permutation and linear-mapping ([7])) through identifying invariant attributes. Specifically, we first compute singular value and eigenvalue invariant matrices from the weight matrices, then derive their corresponding invariant singular values and eigenvalues to construct the model fingerprint. Leveraging the inherent properties of these values, the fingerprint remains both invariant against transformation attacks and robust to downstream modifications such as quantization and fine-tuning.

The similarity computation is performed by a *SimNet*, trained in a few-shot learning paradigm with a limited set of related and unrelated model fingerprints. To enhance generalization, we employ data augmentation techniques including noise injection, row/column deletion, and element masking on the training dataset. This approach ensures robust and accurate similarity comparisons under constrained sample conditions.

Our contributions can be summarized as follows:

1. We present SELF, a weight-based fingerprinting method for LLMs that is inherently resistant to false claim attack. This weight-exclusive methodology eliminates dependency on input samples, thereby preventing false claim of ownership caused by manipulating adversarial inputs.
2. We propose robust fingerprint extraction against transformation attacks. By deriving fingerprints from singular values and eigenvalues of matrices constructed from model weights, our approach leverages their fundamental mathematical properties to ensure uniqueness, scalability, and robustness.
3. Our approach employs a *SimNet* to learn distinctive patterns from the extracted fingerprints. To address data scarcity in the few-shot learning scenario, we implement data augmentation strategies, which enable robust and effective identification of IP infringement.
4. Our comprehensive evaluation across Qwen2.5-7B, Llama2-7B, and their related / unrelated models demonstrates that the proposed method achieves both accurate and robust IP infringement detection. The method maintains its discriminative capability even when subjected to various model modifications, including quantization, pruning, and fine-tuning attacks.

2 Preliminaries

2.1 Attention Mechanism

LLMs widely adopt the Transformer architecture ([13]), with the attention mechanism serving as its core component. The computation of this mechanism can be formulated as:

$$H_{\text{out}} = \text{softmax} \left(\frac{H_{\text{in}} W_Q (H_{\text{in}} W_K)^T}{\sqrt{d}} \right) (H_{\text{in}} W_V) W_O \quad (1)$$

where $H_{\text{in}}, H_{\text{out}} \in \mathbb{R}^{n \times d_{\text{model}}}$ denote the input hidden representations and the self-attention output, respectively, $W_Q, W_K, W_V \in \mathbb{R}^{d_{\text{model}} \times d}$ represent the learnable weight matrices for the Query, Key, and Value matrices, respectively, while $W_O \in \mathbb{R}^{d \times d_{\text{model}}}$ denotes the output weight matrix. Here, n, d and d_{model} correspond to sequence length, projection dimension, and embedding dimension, respectively.

2.2 Transformation Attacks

Model weights are a direct consequence of the specific learning process the model goes through and the data it was trained on, therefore can serve as unique fingerprints for model similarity comparison. However, weights-based fingerprint verification may be evaded by the following transformation attacks, which aim to preserve the model's function behavior but significantly modify the weights ([7]):

Permutation Attack This attack rearranges the weights by permuting the weight matrix. Let $P \in \mathbb{R}^{d_{\text{model}} \times d_{\text{model}}}$ denote an arbitrary permutation matrix. This permutation transformation needs to be applied to the input of the model and corresponding weights:

$$\begin{aligned} \hat{H}_{\text{in}} &= H_{\text{in}} P^T, \\ \hat{W}_Q &= P W_Q, \quad \hat{W}_K = P W_K, \quad \hat{W}_V = P W_V, \quad \hat{W}_O = W_O P^T \end{aligned} \quad (2)$$

As a result, $\hat{H}_{\text{out}} = H_{\text{out}} P^T$. The permutation effect propagates through subsequent layers, making each layer's input and output be permuted with P^T . The original model function can be preserved by applying the same permutation P to the final output.

Linear Mapping Attack Alternatively, a pair of linear transformations can be applied to the attention weights:

$$\hat{W}_Q = W_Q C_1, \quad \hat{W}_K = W_K C_1^{-T}, \quad \hat{W}_V = W_V C_2, \quad \hat{W}_O = C_2^{-1} W_O \quad (3)$$

where $C_1, C_2 \in \mathbb{R}^{d \times d}$ are arbitrary invertible matrices and T denotes the transpose. This linear transformation preserves the attention scores, e.g., $(H_{\text{in}} \hat{W}_Q)(H_{\text{in}} \hat{W}_K)^T = H_{\text{in}} W_Q C_1 C_1^{-1} W_K^T H_{\text{in}}^T = (H_{\text{in}} W_Q)(H_{\text{in}} W_K)^T$, $(H_{\text{in}} \hat{W}_V) \hat{W}_O = (H_{\text{in}} W_V C_2) C_2^{-1} W_O = (H_{\text{in}} W_V) W_O$, leaving the output H_{out} unchanged.

The two attacks highlight a fundamental vulnerability: the model output remains unaffected, while the model weights are altered in ways that invert similarity metrics computed purely on weight comparison.

3 Exploring Singular Values and Eigenvalues as Invariant Fingerprints

Singular values and eigenvalues are fundamental matrix attributes that capture intrinsic properties of a matrix. This section introduces the calculation of the two features and discusses their invariance to transformation attacks.

3.1 Singular Values

Singular values are defined for matrix with any size and describe how much the matrix stretches space along principal mutually orthogonal directions. Any complex matrix $M \in \mathbb{C}^{m \times n}$ admits a singular value decomposition (SVD):

$$M = U \Sigma V^*, \quad (4)$$

where $U \in \mathbb{C}^{m \times m}$ and $V \in \mathbb{C}^{n \times n}$ are unitary matrices. The matrix $\Sigma \in \mathbb{R}^{m \times n}$ is a rectangular diagonal matrix with non-negative real numbers $\sigma_1 \geq \sigma_2 \geq \dots \geq 0$ on the diagonal. These values $\sigma_i = \Sigma_{ii}$ for $i = 1, 2, \dots, \min\{m, n\}$ are uniquely determined by M and are referred to as the *singular values* of M .

Singular values remain unchanged under row, column permutation or any combination of both. Specifically, let $P_1 \in \mathbb{R}^{m \times m}$, $P_2 \in \mathbb{R}^{n \times n}$ be the row and column permutation matrices, respectively, and $\sigma_i(\cdot)$ denote the i_{th} singular value of the corresponding matrix. Since permutation matrices are orthogonal, we have:

$$\sigma_i(M) = \sigma_i(P_1 M) = \sigma_i(M P_2) = \sigma_i(P_1 M P_2). \quad (5)$$

This property ([14]) enables the use of singular values as robust descriptors for model weight matrices, providing resistance to the permutation attacks defined in (2) through the construction of singular value invariant matrix in Section 4.2.

Singular values exhibit stability under small perturbations. Let ΔM denote the perturbations added to matrix M , according to Weyl’s inequality ([14]):

$$|\sigma_i(M + \Delta M) - \sigma_i(M)| \leq \|\Delta M\|_2, \quad (6)$$

where $\|\cdot\|_2$ denotes the spectral norm. This implies that the singular values of a matrix remain approximately unchanged as long as the perturbation magnitude $\|\Delta M\|_2$ is small.

3.2 Eigenvalues

Eigenvalues are defined only for square matrices and describe the scaling factors associated with specific invariant directions (eigenvectors). For a square matrix $N \in \mathbb{C}^{n \times n}$, the eigenvalues $\lambda_1, \dots, \lambda_n$ are defined as the roots of its characteristic polynomial, which are obtained by solving:

$$\det(N - \lambda I) = 0, \quad (7)$$

where \det denotes determinant and I is the identity matrix. If N is diagonalizable, eigenvalues can be more efficiently and stably computed via the following eigenvalue decomposition (EVD):

$$N = Q\Lambda Q^{-1}, \quad (8)$$

where $Q \in \mathbb{C}^{n \times n}$ consists of the linearly independent eigenvectors of N , and $\Lambda \in \mathbb{C}^{n \times n}$ is a diagonal matrix whose diagonal entries $\Lambda_{ii} = \lambda_i$ for $i = 1, 2, \dots, n$ are the eigenvalues of N .

Eigenvalues are invariant under similarity transformations. Let C be an invertible matrix, the operation of transforming a matrix N to $\hat{N} = CNC^{-1}$ is called a similarity transformation. The eigenvalues of \hat{N} can be obtained by solving the roots of

$$\begin{aligned} \det(\hat{N} - \lambda I) &= \det(CNC^{-1} - \lambda I) = \det(CNC^{-1} - \lambda I(CC^{-1})) = \det(CNC^{-1} - C(\lambda I)C^{-1}) \\ &= \det(C(N - \lambda I)C^{-1}) = \det(C)\det(N - \lambda I)\det(C^{-1}) \\ &= \det(C)\det(N - \lambda I)\frac{1}{\det(C)} = \det(N - \lambda I). \end{aligned} \quad (9)$$

Therefore, \hat{N} and N share the same eigenvalues. This property forms the theoretical foundation for defending against the linear mapping attack described in (3) through the construction of eigenvalue invariant matrix in Section 4.2.

Eigenvalues are robust against small perturbations. The Bauer-Fike theorem ([15]) provides a quantitative bound on the sensitivity of eigenvalues under perturbation. Let ΔN denote the perturbation on N and $\lambda_i(\cdot)$ denote the i_{th} eigenvalue of the corresponding matrix. If N is diagonalizable, then for any perturbed matrix $N + \Delta N$ and any $\lambda_i(N + \Delta N)$, there always exists a $\lambda_j(N)$ satisfies:

$$|\lambda_i(N + \Delta N) - \lambda_j(N)| \leq \kappa(Q) \cdot \|\Delta N\|_2, \quad (10)$$

where $\kappa(Q) = \|Q\|_2\|Q^{-1}\|_2$ is the condition number of Q . Thus, if ΔN is small in spectral norm and $\kappa(Q)$ is not too large, the eigenvalues of the perturbed matrix can be close to those of the original. Moreover, a very large $\kappa(Q)$ indicates a high nonnormal N , which can undermine the reliability and convergence of numerical methods ([16]), and thus should be avoided in deep learning systems.

In the context of model fingerprinting, both singular values and eigenvalues can serve as transformation-invariant descriptors, providing robustness against adversarial manipulations of model weights.

4 Methodology

Our method consists of two components: 1) Fingerprint Extraction. This component analyzes the model weights to extract unique and scalable fingerprints by leveraging the properties of singular values and eigenvalues. 2) Similarity Computation. We employ a neural network to learn patterns from the extracted fingerprints, enabling efficient and robust model similarity assessment. The following sections introduce the threat model and these two essential components.

4.1 Threat Model

Our threat model mainly involves three roles: the model owner (original developer or authorized distributor), the model stealer (adversary), and the judge (the trusted third party). The model owner owns the IP of the **target model** (the model to be protected) and maintains white-box access to the model. The model stealer pirates (via extraction, insider theft, or open-source leaks, etc.) the target model and may modify (via fine-tuning, pruning, quantization, or weight transformation attacks, etc.) it to evade IP detection while preserving model functionality. Once the model owner flags a **suspect model** (suspicious to be pirated), he/she could request IP verification procedures by the judge. The judge temporarily obtains white-box access to both the target and suspect models only during the investigation, and its objective is to reliably verify model provenance despite potential adversarial modifications. Crucially, the mechanism must distinguish between: **related models** (derived from the target, even if modified) and **unrelated models** (independently trained), while operating without knowledge of the specific attack employed. Our method aims to provide accurate, robust, and efficient infringement detection for IP forensic scenarios.

4.2 Fingerprint Extraction via Matrix Decomposition

Figure 2 shows the fingerprint extraction pipeline. Given an LLM model, we extract its fingerprint by analyzing the first N_F Transformer block layers. For each layer i , we compute a layer-wise fingerprint \mathcal{F}^i . The overall fingerprint \mathcal{F} of the model can be obtained by aggregating all N_F layer-wise fingerprints.

To extract robust fingerprint, we focus on invariant features derived from the core component of the LLM, i.e., the attention blocks. Compared to other components, the advantage of the attention block lies in (1) High-dimensionality: Attention matrices encodes rich, high-dimensional features (e.g., W_Q, W_K account for $>30\%$ of Llama2-7B’s parameters), while LayerNorm has a much smaller parameter size (e.g., 0.1% of Llama2-7B’s total parameters) and outputs vectors, which limit its utility for SVD- and EVD-based fingerprint extraction. (2) Architectural generality: Attention blocks are universal across transformer variants, while other blocks such as MLPs (e.g., in Mixture of Experts models ([17])) exhibit structural variability that could undermines consistency.

Let $W_Q \in \mathbb{R}^{d_{\text{model}} \times d}$, $W_K \in \mathbb{R}^{d_{\text{model}} \times d}$, $W_V \in \mathbb{R}^{d_{\text{model}} \times d}$ and $W_O \in \mathbb{R}^{d \times d_{\text{model}}}$ denote the query, key, value and output projection weight matrices in a Transformer attention block, where d_{model} is the embedding dimension and d is the projection dimension. As described in Section 2.2, these matrices may be subjected to the permutation and linear mapping attacks of the following form:

$$\hat{W}_Q = PW_Q C_1, \quad \hat{W}_K = PW_K C_1^{-T}, \quad \hat{W}_V = PW_V C_2, \quad \hat{W}_O = C_2^{-1} W_O P^T \quad (11)$$

where $P \in \mathbb{R}^{d_{\text{model}} \times d_{\text{model}}}$ is a permutation matrix, and $C_1, C_2 \in \mathbb{R}^{d \times d}$ are invertible matrices. To counter these attacks, we introduce two transformation-invariant matrices for robust fingerprinting.

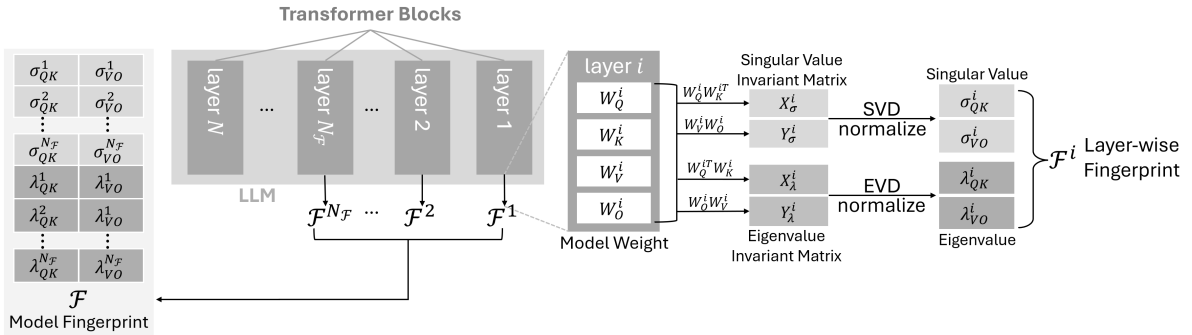


Figure 2: Fingerprint extraction via matrix decomposition. For a given model, we extract its fingerprint using the first N_F Transformer block layers. Specifically, we first compute the fingerprint of each individual layer \mathcal{F}^i and then aggregate the N_F layer-wise fingerprints to form the overall model fingerprint \mathcal{F} . For each layer, we first compute the singular value invariant matrices X_σ^i, Y_σ^i and the eigenvalue invariant matrices X_λ^i, Y_λ^i from the attention weights W_Q^i, W_K^i, W_V^i , and W_O^i . Then, we extract the normalized singular value vector $\sigma_{QK}^i, \sigma_{VO}^i$ and eigenvalue vector $\lambda_{QK}^i, \lambda_{VO}^i$, which together form the fingerprint of layer i .

Singular Value Invariant Matrix We first define matrices X_σ and Y_σ that preserves singular values under the transformation attacks:

$$\begin{aligned} X_\sigma &= W_Q W_K^T \in \mathbb{R}^{d_{\text{model}} \times d_{\text{model}}} \\ Y_\sigma &= W_V W_O \in \mathbb{R}^{d_{\text{model}} \times d_{\text{model}}} \end{aligned} \quad (12)$$

Theorem 1 (Singular Value Invariance). *Under the transformation attack described in (11), the matrices $\hat{X}_\sigma = \hat{W}_Q \hat{W}_K^T$ and $\hat{Y}_\sigma = \hat{W}_V \hat{W}_O$ satisfies:*

$$\begin{aligned} \hat{X}_\sigma &= (PW_Q C_1)(PW_K C_1^{-T})^T = PW_Q C_1 C_1^{-1} W_K^T P^T = PW_Q W_K^T P^T = P X_\sigma P^T \\ \hat{Y}_\sigma &= (PW_V C_2)(C_2^{-1} W_O P^T) = PW_V C_2 C_2^{-1} W_O P^T = PW_V W_O P^T = P Y_\sigma P^T \end{aligned} \quad (13)$$

Since permutation matrices are orthogonal, X_σ and \hat{X}_σ , Y_σ and \hat{Y}_σ are orthogonally equivalent and consequently share the same singular values.

Eigenvalue Invariant Matrix Next, we define matrices X_λ and Y_λ that preserves eigenvalues under the transformation attack:

$$\begin{aligned} X_\lambda &= W_Q^T W_K \in \mathbb{R}^{d \times d} \\ Y_\lambda &= W_O W_V \in \mathbb{R}^{d \times d} \end{aligned} \quad (14)$$

Theorem 2 (Eigenvalue Invariance). *Under the transformation attack described in (11), the matrix $\hat{X}_\lambda = \hat{W}_Q^T \hat{W}_K$ and $\hat{Y}_\lambda = \hat{W}_O^T \hat{W}_V$ satisfies:*

$$\begin{aligned} \hat{X}_\lambda &= (PW_Q C_1)^T (PW_K C_1^{-T}) = C_1^T W_Q^T P^T PW_K C_1^{-T} = C_1^T W_Q^T W_K C_1^{-T} = C_1^T X_\lambda C_1^{-T} \\ \hat{Y}_\lambda &= (C_2^{-1} W_O P^T)(PW_V C_2) = C_2^{-1} W_O P^T PW_V C_2 = C_2^{-1} W_O W_V C_2 = C_2^{-1} Y_\lambda C_2 \end{aligned} \quad (15)$$

This establishes a similarity transformation between X_λ and \hat{X}_λ , Y_λ and \hat{Y}_λ , guaranteeing each matrix pair share identical eigenvalues.

Fingerprint for a Single Layer: Let W_Q^i , W_K^i , W_V^i and W_O^i denote the query, key, value, and output matrices of the i_{th} Transformer block layer. We compute the singular value invariant matrices X_σ^i and Y_σ^i as defined in (12) and the eigenvalue invariant matrices X_λ^i and Y_λ^i as defined in (14). From the two matrices, we extract the following features sorted in descending order by magnitude:

1. the top h singular values of X_σ^i , denoted by vector $\tilde{\sigma}_{QK}^i \in \mathbb{R}^h$,
2. the top h eigenvalues (by magnitude) of X_λ^i , denoted by vector $\tilde{\lambda}_{QK}^i \in \mathbb{R}^h$,
3. the top h singular values of Y_σ^i , denoted by vector $\tilde{\sigma}_{VO}^i \in \mathbb{R}^h$,
4. the top h eigenvalues (by magnitude) of Y_λ^i , denoted by vector $\tilde{\lambda}_{VO}^i \in \mathbb{R}^h$,

then each vector is normalized to unit L_2 norm, e.g., $\sigma_{QK}^i = \frac{\tilde{\sigma}_{QK}^i}{\|\tilde{\sigma}_{QK}^i\|_2}$, and the fingerprint for layer i is then defined with the normalized vectors as $\mathcal{F}^i = [\sigma_{QK}^i, \lambda_{QK}^i, \sigma_{VO}^i, \lambda_{VO}^i]^T \in \mathbb{R}^{4 \times h}$.

Fingerprint for the Whole Model: As studied by [10], lower-layer (near to the input) weights tend to be more robust against fine-tuning or task-specific adaptations. Therefore, we extract fingerprints from the first $N_{\mathcal{F}}$ Transformer layers. The full model fingerprint is obtained by stacking all singular and eigenvalue vectors in the following order:

$$\begin{aligned} \mathcal{F} &= [\sigma_{QK}^1, \sigma_{QK}^2, \dots, \sigma_{QK}^{N_{\mathcal{F}}}, \lambda_{QK}^1, \lambda_{QK}^2, \dots, \lambda_{QK}^{N_{\mathcal{F}}}, \\ &\quad \sigma_{VO}^1, \sigma_{VO}^2, \dots, \sigma_{VO}^{N_{\mathcal{F}}}, \lambda_{VO}^1, \lambda_{VO}^2, \dots, \lambda_{VO}^{N_{\mathcal{F}}}]^T \in \mathbb{R}^{4N_{\mathcal{F}} \times h} \end{aligned} \quad (16)$$

This fingerprint matrix \mathcal{F} captures intrinsic structural information from multiple attention layers, while remaining robust to the weight transformation attacks.

4.3 Fingerprint Similarity Computation via Neural Network

To determine whether a suspect model is a derived variant of the target model, we adopt a residual network ([18]) based fingerprint similarity network, denoted as $\text{SimNet} : \mathbb{R}^{4N_F \times h} \rightarrow [0, 1]$, which maps a model fingerprint $\mathcal{F} \in \mathbb{R}^{4N_F \times h}$ to a similarity score ranges from 0 to 1.

To train SimNet , we firstly construct a labeled training set: $\mathcal{D}_{\text{train}} = \{(\mathcal{F}_i, y_i)\}_{i=1}^n$, where $y_i = 1$ if \mathcal{F}_i originates from the target model or a related model, and $y_i = 0$ if it is from an unrelated model.

Due to limited training samples, we train SimNet using a few-shot learning scheme, employing data augmentation to expand $\mathcal{D}_{\text{train}}$. Specifically, we augment $\mathcal{D}_{\text{train}}$ by applying Gaussain noise, row deletion, column deletion, and random masking to W_Q, W_K, W_V and W_O of the first N_F Transformer layers.

Specifically, we modify the attention weights in the first N_F Transformer layers as follows:

1. **Gaussian Noise:** Add random Gaussian noise sampled i.i.d. from the standard normal distribution— $\mathbf{N}_Q, \mathbf{N}_K, \mathbf{N}_V, \mathbf{N}_O \sim \mathcal{N}(0, 1)$ —to the weight matrices with strength α :

$$\begin{aligned}\tilde{W}_Q &= W_Q + \alpha \mathbf{N}_Q, & \tilde{W}_K &= W_K + \alpha \mathbf{N}_K, \\ \tilde{W}_V &= W_V + \alpha \mathbf{N}_V, & \tilde{W}_O &= W_O + \alpha \mathbf{N}_O.\end{aligned}\tag{17}$$

2. **Row Deletion:** Randomly select a subset of indices $\mathcal{I}_r \subset \{1, \dots, d_{\text{model}}\}$ with $|\mathcal{I}_r| = n_r$, and delete the corresponding rows from W_Q, W_K , and W_V , and delete the corresponding columns from W_O .
3. **Column Deletion:** Randomly select a subset of indices $\mathcal{I}_c \subset \{1, \dots, d\}$ with $|\mathcal{I}_c| = n_c$, and delete the corresponding columns from W_Q, W_K , and W_V , and delete the corresponding rows from W_O .
4. **Random Masking:** Mask the weight matrices based on a predefined threshold r and random noise matrix sampled i.i.d from a uniform distribution— $\mathbf{N}_Q, \mathbf{N}_K, \mathbf{N}_V, \mathbf{N}_O \sim \mathcal{U}(0, 1)^{d_{\text{model}} \times d}$:

$$\begin{aligned}\tilde{W}_Q(i, j) &= W_Q(i, j) \odot \mathbb{M}[\mathbf{N}_Q(i, j) \geq r], \\ \tilde{W}_K(i, j) &= W_K(i, j) \odot \mathbb{M}[\mathbf{N}_K(i, j) \geq r], \\ \tilde{W}_V(i, j) &= W_V(i, j) \odot \mathbb{M}[\mathbf{N}_V(i, j) \geq r], \\ \tilde{W}_O(i, j) &= W_O(i, j) \odot \mathbb{M}[\mathbf{N}_O^T(i, j) \geq r].\end{aligned}\tag{18}$$

where \odot is the element-wise multiplication and $\mathbb{M}[\mathbf{N} > r]$ is a binary matrix where each element is 1 if $N_{i,j} \geq r$, and 0 otherwise.

The augmented weights $(\tilde{W}_Q, \tilde{W}_K, \tilde{W}_V, \tilde{W}_O)$ are used to compute the invariant matrices $\tilde{X}_\sigma, \tilde{X}_\lambda, \tilde{Y}_\sigma$, and \tilde{Y}_λ , from which we derive the augmented fingerprint $\tilde{\mathcal{F}}$. The final training dataset is $\tilde{\mathcal{D}}_{\text{train}} = \mathcal{D}_{\text{train}} \cup \left\{(\tilde{\mathcal{F}}_j, y_j)\right\}_{j=1}^{\tilde{n}}$, where $\tilde{\mathcal{F}}_j$ denotes an augmented fingerprint generated from a model with label y_j , and \tilde{n} is the number of augmented fingerprint samples.

With the augmented dataset $\tilde{\mathcal{D}}_{\text{train}}$, SimNet for the target model T can be trained. Given a suspect model S and a predefined similarity threshold $\tau \in [0, 1]$, if $\text{SimNet}(\mathcal{F}_S) > \tau$, S is considered potentially related to the target model due to the high similarity score. Otherwise, the suspect model is detected as unrelated models.

5 Experiments

Experiment Settings: we extract fingerprints from the first $N_F = 8$ layers, using the top $h = 256$ singular values and eigenvalues, resulting in fingerprint size of 32×256 . For each target model, the training dataset for SimNet includes the extracted fingerprints of the model itself, one of its fine-tuned offspring and three unrelated models. Model architecture and training details of SimNet can be found in Appendix E.

5.1 Effectiveness Verification

We use Qwen2.5-7B and Llama2-7B as target models to evaluate the effectiveness of SELF, and their publicly available offsprings are used as related models. For unrelated models, we select 10 independent open-source models with diverse architectures and parameter sizes ranging from 800M to 7B. As shown in Table 1, the similarity score of related models

Table 1: Fingerprint Similarity (Target Models: Qwen2.5-7B and Llama2-7B)

Qwen2.5-7B Unrelated		Qwen2.5-7B Related		Llama2-7B Unrelated		Llama2-7B Related	
Model	Score	Model	Score	Model	Score	Model	Score
Mistral-7B-V0.3	0.0050	Fine-tuned Variants		Mistral-7B-V0.3	0.0050	Fine-tuned Variants	
Llama2-7B	0.0020	Qwen2.5-7B-Instruct	0.9950	Qwen1.5-7B	0.2902	Llama-2-7B-Chat	0.9950
Baichuan2-7B	0.0009	Qwen2.5-Math-7B	0.9979	Baichuan2-7B	0.1862	CodeLlama-7B	0.9641
InternLM2.5-7B	0.0139	Qwen2.5-Coder-7B	0.9910	InternLM2.5-7B	0.0050	Llemma-7B	0.9699
GPT2-Large	0.0050	TableGPT2-7B	0.9944	GPT2-Large	0.2372	Pruned Variants	
Cerebras-GPT-1.3B	0.0011	Qwen2.5-7B-Medicine	0.9950	Cerebras-GPT-1.3B	0.2874	Sheared-Llama-2-7B	0.9917
ChatGLM2-6B	0.0091	Qwen2.5-7B-abliterated-v2	0.9950	ChatGLM2-6B	0.0057	SparseLlama-2-7B	0.9941
OPT-6.7B	0.0005	Quantized Variants		OPT-6.7B	0.0009	Quantized Variants	
Pythia-6.9B	0.0156	Qwen2.5-7B-4bit	0.9950	Pythia-6.9B	0.0002	Llama2-7B-4bit	0.9950
MPT-7B	0.0050	Qwen2.5-7B-8bit	0.9950	MPT-7B	0.0050	Llama2-7B-8bit	0.9950

High similarity (>0.5) means potential IP infringement.

are greater than 0.9 while those for unrelated models are less than 0.3, demonstrating that our method can effectively discriminate between related and unrelated models.

It is important to note that Qwen2.5-7B employs Grouped-Query Attention (GQA), which groups multiple query heads to share a single key-value head pair. This architecture introduces a dimensionality mismatch with previous definition in Sec. 2.1, as the number of key and value heads is smaller than that of the query heads. To resolve this compatibility issue, we conceptually broadcast the shared weights in W_K and W_V to align with the number of query heads. This replication functions as a structured weight-sharing constraint, ensuring GQA-based models like Qwen2.5-7B to be seamlessly integrated into our fingerprinting framework.

To provide intuitive performance of the fingerprint \mathcal{F} 's discriminability, we further include in the Appendix D the fingerprint distance between the above models and three DeepSeek-R1 ([19]) distilled models versus their base models, demonstrating effectiveness across diverse architectures.

5.2 Robustness Verification

We assess the robustness of SELF by evaluating its resilience against carefully crafted fine-tuning attacks and model pruning. A robust fingerprint should maintain a high similarity score while preserving model performance under such modification.

5.2.1 Robustness against Fine-tuning Attack

An attacker may fine-tune the stolen model to evade IP detection by intentionally adjusting model parameters so that the extracted fingerprint \mathcal{F}_S is deviated from the original \mathcal{F}_T . Formally, this is achieved by optimizing the attack loss $L_{\text{attack}} = 1/(\|\mathcal{F}_M - \mathcal{F}_T\|_2 + \epsilon)$, where \mathcal{F}_M is the fingerprint of the stolen model and $\epsilon = 10^{-9}$ serves as a small constant for numerical stability. Moreover, an attacker may also try to use actual dataset to maintain the model's performance, optimizing a combined objective incorporating both the attack loss and the dataset loss, i.e., $l_1 L_{\text{attack}} + l_2 L_{\text{data}}$. In the experiment, we use the cross-entropy loss on WikiText2 dataset as L_{data} . To keep the two loss functions on the same scale, we adopt $l_1 = 0.1, l_2 = 1$.

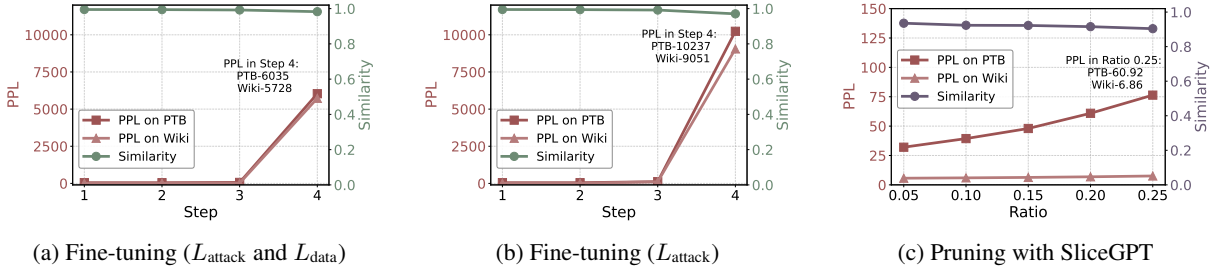


Figure 3: Fingerprint similarity and PPL change of Llama2-7B under different attacks. (a) and (b) show the results under fine-tuning attacks. (c) shows the results under SliceGPT pruning. Since State-of-The-Art LSTM achieves PPL smaller than 60 on PTB dataset ([20]), we consider a PPL of 60 or higher as “unacceptable” for larger models like transformer.

We implemented this fine-tuning attack on the Llama2-7B model, employing a learning rate of 5×10^{-3} and evaluating the model's performance change. To account for randomness, we averaged the results from four random seeds (10,

42, 99, 1024). We analyze both fingerprint similarity and model performance degradation, measuring the latter using perplexity (PPL) on WikiText2 ([21]) and PTB ([22]) benchmarks. A lower PPL indicates better performance. Figures 3a and 3b show that even if the target model has been extensively fine-tuned to have significantly degraded performance, the fingerprint similarity still remains high, demonstrating the robustness of our scheme against such fine-tuning attacks.

5.2.2 Robustness against Pruning

An attacker may attempt to disrupt the fingerprint by increasing pruning levels. Therefore, we examine the impact of varying pruning ratios on fingerprint robustness. Specifically, we prune Llama2-7B with SliceGPT ([23]), a structured pruning by removing entire rows or columns from LLM weight matrices while minimizing performance degradation, and analyze fingerprint similarity and performance variations across different pruning levels.

Figure 3c shows that the PPL of Llama2-7B on PTB dataset deteriorates beyond that of an LSTM baseline when the pruning ratio reaches 0.25, but our method maintains a high fingerprint similarity (> 0.9) for infringement detection. We provide more detection results for pruned model instances in Appendix C.

5.3 Comparison

This section benchmarks SELF against published structural fingerprinting methods for LLMs, including PCS and ICS proposed by [7], and REEF proposed by [8]. A detailed introduction of these related works are presented in Appendix A.

Table 2 compares the mechanism and fingerprint size against various modifications across these LLM fingerprinting methods. SELF employs SVD- and EVD- based invariant matrix decomposition, requiring only partial parameters for fingerprint extraction and achieving a compact fingerprint size of approximately 10^3 elements (for any model size). Compared to prior works that extract fingerprints ranging from 10^4 to 10^9 elements (for a 7B model), SELF significantly reduces storage overhead while preserving discriminative capability.

Table 2: Comparison of Mechanism and Fingerprint Size

Method		Requirement	Fingerprint size
PCS	Parameter’s vector direction	All parameters	$\text{parameter_num} (\sim 10^9)$
ICS	Invariant terms’ similarity	Partial parameters and input	$3 \times \text{selected_layer_num} \times (\text{sample_num})^2 (\sim 10^9)$
REEF	Representation’s CKA	Partial parameters and input	$\text{sample_num} \times d_{\text{model}} (\sim 10^4 - 10^6)$
SELF	Invariant matrix decomposition	Partial parameters	$4N_{\mathcal{F}} \times h (\sim 10^3)$

CKA: Centered Kernel Alignment

Table 3 compares robustness against various attacks. By leveraging intrinsic model weights and eliminating input dependency, SELF is inherently robust against false claim attacks. Its SVD- and EVD- constructed fingerprints also provide strong attack resilience against linear mapping and permutation attacks due to their fundamental mathematical invariance properties. Besides, the proposed method is also evaluated to be robust against fine-tuning and pruning attacks, highlighting its effectiveness in practical deployment scenarios. A quantitative comparison between SELF and these methods are further provided in Appendix C.

Table 3: Comparison of Robustness Against Various Attacks

Methods	Fine-tuning	Pruning	Permutation Attack	Linear-mapping Attack	False Claim Attack
PCS	✓				✓
ICS	✓		✓	✓	
REEF	✓	✓	✓	✓	
SELF	✓	✓	✓	✓	✓

✓ indicates resilience against this attack.

6 Conclusion

This paper presents SELF, a weight-based fingerprinting method that eliminates input dependency, preventing false claim attacks. By extracting fingerprints utilizing singular values and eigenvalues, we leverage their mathematical properties to guarantee uniqueness, scalability, and robustness. A *SimNet* further learns distinctive fingerprint patterns, enabling effective IP infringement detection. Our approach thus serves as a reliable tool for LLM model IP protection.

References

- [1] Arun James Thirunavukarasu, Darren Shu Jeng Ting, Kabilan Elangovan, Laura Gutierrez, Ting Fang Tan, and Daniel Shu Wei Ting. Large language models in medicine. *Nature medicine*, 29(8):1930–1940, 2023.
- [2] Sarah Fakhoury, Aaditya Naik, Georgios Sakas, Saikat Chakraborty, and Shuvendu K Lahiri. Llm-based test-driven interactive code generation: User study and empirical evaluation. *IEEE Transactions on Software Engineering*, 2024.
- [3] Yue Zheng, Chip-Hong Chang, Shih-Hsu Huang, Pin-Yu Chen, and Stjepan Picek. An overview of trustworthy ai: advances in ip protection, privacy-preserving federated learning, security verification, and gai safety alignment. *IEEE Journal on Emerging and Selected Topics in Circuits and Systems*, 2024.
- [4] Ruisi Zhang, Shehzeen Samarah Hussain, Paarth Neekhara, and Farinaz Koushanfar. {REMARK-LLM}: A robust and efficient watermarking framework for generative large language models. In *33rd USENIX Security Symposium (USENIX Security 24)*, pages 1813–1830, 2024.
- [5] Jiashu Xu, Fei Wang, Mingyu Ma, Pang Wei Koh, Chaowei Xiao, and Muhao Chen. Instructional fingerprinting of large language models. In *Proceedings of the 2024 Conference of the North American Chapter of the Association for Computational Linguistics: Human Language Technologies (Volume 1: Long Papers)*, pages 3277–3306, 2024.
- [6] Martin Gubri, Dennis Ulmer, Hwaran Lee, Sangdoo Yun, and Seong Joon Oh. Trap: Targeted random adversarial prompt honeypot for black-box identification. In *Findings of the Association for Computational Linguistics ACL 2024*, pages 11496–11517, 2024.
- [7] Boyi Zeng, Lizheng Wang, Yuncong Hu, Yi Xu, Chenghu Zhou, Xinbing Wang, Yu Yu, and Zhouhan Lin. Huref: Human-readable fingerprint for large language models. *Advances in Neural Information Processing Systems*, 37:126332–126362, 2024.
- [8] Jie Zhang, Dongrui Liu, Chen Qian, Linfeng Zhang, Yong Liu, Yu Qiao, and Jing Shao. REEF: Representation encoding fingerprints for large language models. In *The Thirteenth International Conference on Learning Representations*, 2025.
- [9] Zehao Wu, Yanjie Zhao, and Haoyu Wang. Gradient-based model fingerprinting for llm similarity detection and family classification, 2025.
- [10] Yue Zheng, Si Wang, and Chip-Hong Chang. A dnn fingerprint for non-repudiable model ownership identification and piracy detection. *IEEE Transactions on Information Forensics and Security*, 17:2977–2989, 2022.
- [11] Jian Liu, Rui Zhang, Sebastian Szyller, Kui Ren, and N Asokan. False claims against model ownership resolution. In *33rd USENIX Security Symposium (USENIX Security 24)*, pages 6885–6902, 2024.
- [12] Shuo Shao, Haozhe Zhu, Hongwei Yao, Yiming Li, Tianwei Zhang, Zhan Qin, and Kui Ren. Fit-print: Towards false-claim-resistant model ownership verification via targeted fingerprint, 2025.
- [13] Ashish Vaswani, Noam Shazeer, Niki Parmar, Jakob Uszkoreit, Llion Jones, Aidan N Gomez, Łukasz Kaiser, and Illia Polosukhin. Attention is all you need. *Advances in neural information processing systems*, 30, 2017.
- [14] Joel N Franklin. *Matrix theory*. Courier Corporation, 2000.
- [15] Friedrich L Bauer and Charles T Fike. Norms and exclusion theorems. *Numerische mathematik*, 2(1):137–141, 1960.
- [16] Françoise Chaitin-Chatelin. Is nonnormality a serious computational difficulty in practice? In *Quality of Numerical Software: Assessment and enhancement*, pages 300–314. Springer, 1997.
- [17] Noam Shazeer, Azalia Mirhoseini, Krzysztof Maziarz, Andy Davis, Quoc Le, Geoffrey Hinton, and Jeff Dean. Outrageously large neural networks: The sparsely-gated mixture-of-experts layer. In *International Conference on Learning Representations*, 2017.
- [18] Kaiming He, Xiangyu Zhang, Shaoqing Ren, and Jian Sun. Deep residual learning for image recognition. In *Proceedings of the IEEE Conference on Computer Vision and Pattern Recognition (CVPR)*, June 2016.
- [19] DeepSeek-AI, Daya Guo, Dejian Yang, Haowei Zhang, Junxiao Song, Ruoyu Zhang, Runxin Xu, Qihao Zhu, Shirong Ma, Peiyi Wang, Xiao Bi, Xiaokang Zhang, Xingkai Yu, Yu Wu, Z. F. Wu, Zhibin Gou, Zhihong Shao, Zhuoshu Li, Ziyi Gao, Aixin Liu, Bing Xue, Bingxuan Wang, Bochao Wu, Bei Feng, Chengda Lu, Chenggang Zhao, Chengqi Deng, Chenyu Zhang, Chong Ruan, Damai Dai, Deli Chen, Dongjie Ji, Erhang Li, Fangyun Lin, Fucong Dai, Fuli Luo, Guangbo Hao, Guanting Chen, Guowei Li, H. Zhang, Han Bao, Hanwei Xu, Haocheng Wang, Honghui Ding, Huajian Xin, Huazuo Gao, Hui Qu, Hui Li, Jianzhong Guo, Jia Shi Li, Jiawei Wang, Jingchang Chen, Jingyang Yuan, Junjie Qiu, Junlong Li, J. L. Cai, Jiaqi Ni, Jian Liang, Jin Chen, Kai Dong, Kai Hu, Kaige Gao, Kang Guan, Kexin Huang, Kuai Yu, Lean Wang, Lecong Zhang, Liang Zhao, Litong Wang, Liyue

- Zhang, Lei Xu, Leyi Xia, Mingchuan Zhang, Minghua Zhang, Minghui Tang, Meng Li, Miaojun Wang, Mingming Li, Ning Tian, Panpan Huang, Peng Zhang, Qiancheng Wang, Qinyu Chen, Qiushi Du, Ruiqi Ge, Ruisong Zhang, Ruizhe Pan, Runji Wang, R. J. Chen, R. L. Jin, Ruyi Chen, Shanghao Lu, Shangyan Zhou, Shanhuang Chen, Shengfeng Ye, Shiyu Wang, Shuiping Yu, Shunfeng Zhou, Shuting Pan, S. S. Li, Shuang Zhou, Shaoqing Wu, Shengfeng Ye, Tao Yun, Tian Pei, Tianyu Sun, T. Wang, Wangding Zeng, Wanxia Zhao, Wen Liu, Wenfeng Liang, Wenjun Gao, Wenqin Yu, Wentao Zhang, W. L. Xiao, Wei An, Xiaodong Liu, Xiaohan Wang, Xiaokang Chen, Xiaotao Nie, Xin Cheng, Xin Liu, Xin Xie, Xingchao Liu, Xinyu Yang, Xinyuan Li, Xuecheng Su, Xuheng Lin, X. Q. Li, Xiangyue Jin, Xiaojin Shen, Xiaosha Chen, Xiaowen Sun, Xiaoxiang Wang, Xinnan Song, Xinyi Zhou, Xianzu Wang, Xinxia Shan, Y. K. Li, Y. Q. Wang, Y. X. Wei, Yang Zhang, Yanhong Xu, Yao Li, Yao Zhao, Yaofeng Sun, Yaohui Wang, Yi Yu, Yichao Zhang, Yifan Shi, Yiliang Xiong, Ying He, Yishi Piao, Yisong Wang, Yixuan Tan, Yiyang Ma, Yiyuan Liu, Yongqiang Guo, Yuan Ou, Yudian Wang, Yue Gong, Yuheng Zou, Yujia He, Yunfan Xiong, Yuxiang Luo, Yuxiang You, Yuxuan Liu, Yuyang Zhou, Y. X. Zhu, Yanhong Xu, Yanping Huang, Yaohui Li, Yi Zheng, Yuchen Zhu, Yunxian Ma, Ying Tang, Yukun Zha, Yuting Yan, Z. Z. Ren, Zehui Ren, Zhangli Sha, Zhe Fu, Zhean Xu, Zhenda Xie, Zhengyan Zhang, Zhewen Hao, Zhicheng Ma, Zhigang Yan, Zhiyu Wu, Zihui Gu, Zijia Zhu, Zijun Liu, Zilin Li, Ziwei Xie, Ziyang Song, Zizheng Pan, Zhen Huang, Zhipeng Xu, Zhongyu Zhang, and Zhen Zhang. Deepseek-r1: Incentivizing reasoning capability in llms via reinforcement learning, 2025.
- [20] Stephen Merity, Nitish Shirish Keskar, and Richard Socher. Regularizing and optimizing LSTM language models. In *International Conference on Learning Representations*, 2018.
- [21] Stephen Merity, Caiming Xiong, James Bradbury, and Richard Socher. Pointer sentinel mixture models, 2016.
- [22] Mitchell P. Marcus, Beatrice Santorini, and Mary Ann Marcinkiewicz. Building a large annotated corpus of English: The Penn Treebank. *Computational Linguistics*, 19(2):313–330, 1993.
- [23] Saleh Ashkboos, Maximilian L. Croci, Marcelo Gennari do Nascimento, Torsten Hoeffler, and James Hensman. SliceGPT: Compress large language models by deleting rows and columns. In *The Twelfth International Conference on Learning Representations*, 2024.
- [24] Hengyuan Xu, Liyao Xiang, Xingjun Ma, Borui Yang, and Baochun Li. Hufu: A modality-agnostic watermarking system for pre-trained transformers via permutation equivariance. *CoRR*, 2024.
- [25] Shuai Li, Kejiang Chen, Kunsheng Tang, Jie Zhang, Weiming Zhang, Nenghai Yu, and Kai Zeng. Turning your strength into watermark: Watermarking large language model via knowledge injection, 2024.
- [26] Linyang Li, Botian Jiang, Pengyu Wang, Ke Ren, Hang Yan, and Xipeng Qiu. Watermarking llms with weight quantization. In *Findings of the Association for Computational Linguistics: EMNLP 2023*, pages 3368–3378, 2023.
- [27] Sumanth Dathathri, Abigail See, Sumedh Ghaisas, Po-Sen Huang, Rob McAdam, Johannes Welbl, Vandana Bachani, Alex Kaskasoli, Robert Stanforth, Tatiana Matejovicova, et al. Scalable watermarking for identifying large language model outputs. *Nature*, 634(8035):818–823, 2024.
- [28] John Kirchenbauer, Jonas Geiping, Yuxin Wen, Jonathan Katz, Ian Miers, and Tom Goldstein. A watermark for large language models. In *International Conference on Machine Learning*, pages 17061–17084. PMLR, 2023.
- [29] Vinu Sankar Sadasivan, Aounon Kumar, Sriram Balasubramanian, Wenxiao Wang, and Soheil Feizi. Can ai-generated text be reliably detected?, 2025.
- [30] Aiwei Liu, Leyi Pan, Xuming Hu, Shiao Meng, and Lijie Wen. A semantic invariant robust watermark for large language models. In *The Twelfth International Conference on Learning Representations*, 2024.
- [31] Dmitri Iourovitski, Sanat Sharma, and Rakshak Talwar. Hide and seek: Fingerprinting large language models with evolutionary learning, 2024.
- [32] Dario Pasquini, Evgenios M. Kornaropoulos, and Giuseppe Ateniese. Llmmap: Fingerprinting for large language models, 2025.
- [33] Stephanie Lin, Jacob Hilton, and Owain Evans. Truthfulqa: Measuring how models mimic human falsehoods. In *Proceedings of the 60th Annual Meeting of the Association for Computational Linguistics (Volume 1: Long Papers)*, pages 3214–3252, 2022.
- [34] Niloofar Mireshghallah, Hyunwoo Kim, Xuhui Zhou, Yulia Tsvetkov, Maarten Sap, Reza Shokri, and Yejin Choi. Can llms keep a secret? testing privacy implications of language models via contextual integrity theory, 2024.
- [35] Jiaming Ji, Donghai Hong, Borong Zhang, Boyuan Chen, Juntao Dai, Boren Zheng, Tianyi Qiu, Jiayi Zhou, Kaile Wang, Boxuan Li, Sirui Han, Yike Guo, and Yaodong Yang. Pku-saferllm: Towards multi-level safety alignment for llms with human preference, 2025.

- [36] Thomas Hartvigsen, Saadia Gabriel, Hamid Palangi, Maarten Sap, Dipankar Ray, and Ece Kamar. Toxigen: A large-scale machine-generated dataset for adversarial and implicit hate speech detection. In *Proceedings of the 60th Annual Meeting of the Association for Computational Linguistics (Volume 1: Long Papers)*, pages 3309–3326, 2022.
- [37] Richard Socher, Alex Perelygin, Jean Wu, Jason Chuang, Christopher D Manning, Andrew Y Ng, and Christopher Potts. Recursive deep models for semantic compositionality over a sentiment treebank. In *Proceedings of the 2013 conference on empirical methods in natural language processing*, pages 1631–1642, 2013.

Appendix

A Related Works

Current model IP infringement detection methods mainly use watermarking or fingerprinting. Watermarking embeds identifiable features into the target models, while fingerprinting extracts unique identifiers without modifying the model, thus avoiding retraining and performance degradation.

Watermarking Watermarking approaches for LLMs primarily operate through two paradigms: model-centric watermarking and sampling-centric watermarking.

Model-centric techniques focus on embedding watermarks by modifying the model’s architecture, parameters, or training process, typically involve fine-tuning or quantization strategies. For instance, [24] leverages the permutation equivariance property of Transformers to embed watermarks by fine-tuning on strategically permuted data samples. Alternatively, [25] introduces a knowledge injection approach where the watermark is carried through learned knowledge, while [26] implements watermarking during the model quantization process. These approaches typically require additional retraining or fine-tuning cost.

Sampling-centric methods embed watermarks by modifying the token sampling process or latent representations during text generation. These approaches do not alter the model’s parameters but instead tweak the decoding strategy or latent space. [4] presents REMARK-LLM, a framework that encodes both generated text and binary messages into latent space before transforming tokens into sparse distributions. [27] develops Tournament sampling, a modified sampling algorithm for watermark embedding. The KGW method ([28]) employs a “green list” approach, preferentially selecting predetermined tokens during generation. However, such watermarking scheme remains susceptible to editing and spoofing attacks [29]. To mitigate this issue, [30] proposes a semantic invariant watermarking (SIR) method that generates watermarked tokens based on sentence-level embeddings. For sampling-centric approaches, additional post-processing may be required to verify watermarks.

Fingerprinting Existing LLM fingerprinting methods encompass either behavior fingerprinting and structure fingerprinting. Behavior fingerprinting focus on identifying LLMs by analyzing their output characteristics or input-response patterns. These methods leverage the unique behavior signatures that emerge from how models respond to specific inputs or adversarial prompts. [6] employs adversarial suffixes to elicit model-specific responses, while [31] develops an evolutionary strategy using one LLM to identify distinctive features of others. [32] utilizes carefully designed queries to detect specific model versions. As these methods rely on observable input-output interactions, they are effective for black-box scenarios but remain vulnerable to attacks like false claim attack [11].

Structural fingerprinting methods analyze internal parameters or activation patterns. These methods exploit the unique structural properties of a model’s architecture or training dynamics. [7] proposes HuRef, a human-readable fingerprint based on the stability of LLM parameter vector directions after pretraining convergence. While these vector directions demonstrate resilience to subsequent training, they remain vulnerable to direct weight manipulations such as permutation and linear mapping. To address this limitation, the authors develop three rearrangement-invariant fingerprint terms. [8] introduces REEF, a representation-based fingerprinting method employing Centered Kernel Alignment (CKA) to compute similarity score. [9] presents TensorGuard, a framework extracting gradient-based signatures by analyzing their internal gradient responses across tensor layers to random input perturbations. However, these fingerprinting techniques also exhibit vulnerability to false claim attacks [11] due to their inherent reliance on input engagement.

B Implementation of False Claim Attack on HuRef

In this section, we simulate an adversarial scenario by conducting false claim attacks against the HuRef ([7])’s ICS method. Figure 4 shows the critical path in the similarity scoring mechanism of HuRef. Given an LLM, HuRef uses the input embeddings E together with the model weights to compute invariant terms I , which serve as the model’s fingerprint. The cosine similarity of I is then used to detect potential IP infringement. In addition, HuRef encodes I into feature vector v and generate human-readable fingerprints (images), where visual similarity indicates related models.

We envisioned an attack scenario where the malicious actor (a malicious owner or model stealer) aims to falsely claim the ownership of an unrelated model to his/her target or stolen model. To this end, the attacker carefully crafts input tokens so that, when the feature vector is computed following HuRef, the unrelated model yield high similarity to attacker’s model, leading to deceptive readable fingerprints. Since the embedding step ($X \rightarrow E$) is not differentiable, we choose the genetic algorithm to implement the attack. Specifically, we treat a token as a gene and a input as an individual, and define the fitness as the similarity between the feature vectors computed by the two models given that input. In each generation, we apply random gene mutations (i.e., token substitutions) to the population of input individuals and select those with the highest fitness (i.e., highest feature vector similarity) for crossover to produce a new population. After several generations, the input with the highest fitness in the final population is selected as the false claim input. Such an attack only manipulates the input without altering the model itself.

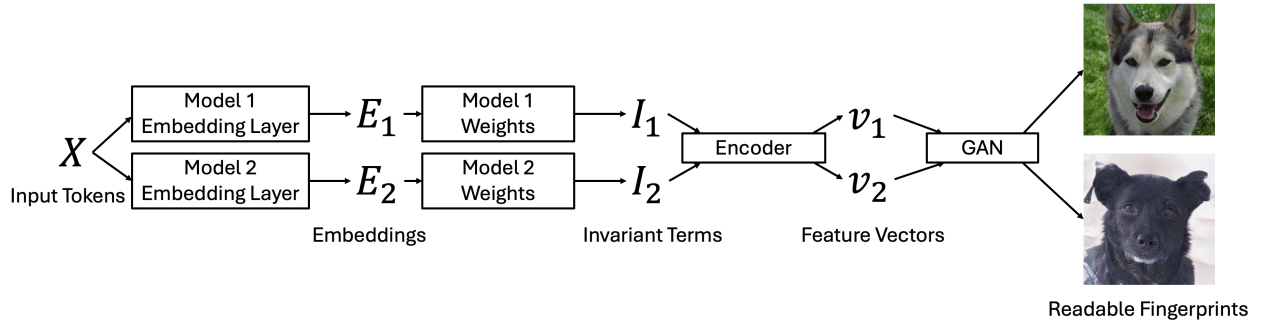
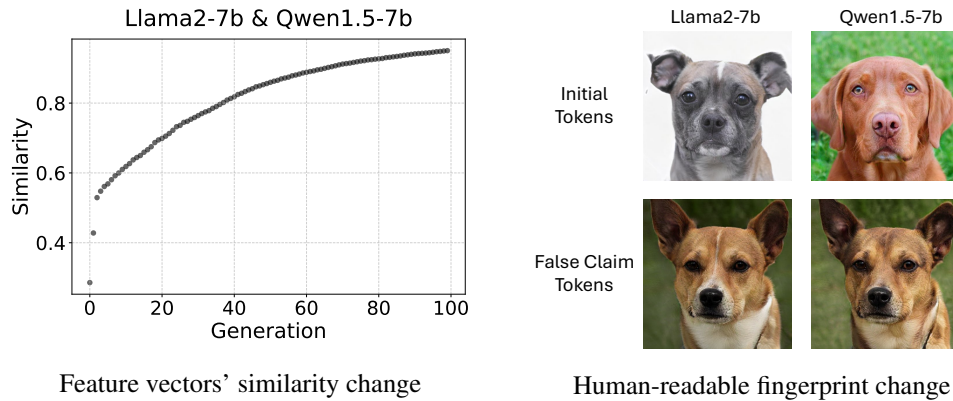


Figure 4: HuRef calculation process in our false claim attack

In our experiment, we assume the attacker holds Llama2-7B and he/she wants to deliberately claim the ownership of an unrelated model Qwen1.5-7B. By feeding the two models with a carefully crafted input obtained as described above, their feature vector similarity increased from 28% to 95% after 100 generations, leading to a false claim of model piracy. Moreover, the generated readable fingerprints shifted from being completely unrelated to appearing similar when using the false claim tokens, indicating that fingerprint similarity can be artificially induced.



C Quantitative Comparison with Previous Methods

To further demonstrate the numerical superiority of our method, this section presents quantitative comparisons between our method with previous approaches. Follow [8], we present the IP detection results on publicly available models in Table 4 to Table 7. The performance (similarity) for previous methods are sourced directly from [8], which conducted comprehensive comparison with existing works and reported the corresponding data. For consistency, we reuse these reported values to benchmark our method against the state of the art. False judgments are highlighted in gray.

Comparison of fine-tuned variants detectability Table 4 compares SELF with existing methods for detecting fine-tuned related models. The target model is Llama2-7B and its six fine-tuned variants are set as suspect models, fine-tuned on datasets ranging from 5M to 700B tokens. It can be observed that even after the target model is fine-tuned on large-scale data, SELF still identifies related models with a similarity score above 0.9, while PCS and ICS failed to detect some fine-tuned related models.

Table 4: Comparison of fingerprint similarity score on Llama2-7B fine-tuned models

	Fine-tuning					
	Llama-2-finance-7B (5M Tokens)	Vicuna-1.5-7B (370M Tokens)	Wizardmath-7B (1.8B Tokens)	Chinesellama-2-7B (13B Tokens)	Codellama-7B (500B Tokens)	Llemma-7B (700B Tokens)
PCS	0.9979	0.9985	0.0250	0.0127	0.0105	0.0098
ICS	0.9952	0.9949	0.9994	0.4996	0.2550	0.2257
REEF	0.9950	0.9985	0.9979	0.9974	0.9947	0.9962
SELF	0.9948	0.9949	0.9949	0.9947	0.9641	0.9699

Comparison of pruned variants detectability Tables 5 and 6 compares SELF with existing methods for detecting pruned related models. Llama-2-7B is used as the target model and its pruned variants as suspect models. Table 5 lists the fingerprint similarity scores of Llama-2-7B’s structured pruned models and Table 6 reports those of unstructured pruned models. The results show that SELF can reliably detect pruned related models with high similarity.

Table 5: Comparison of fingerprint similarity score on Llama2-7B structured pruned models

	Structured Pruning					
	Sheared-Llama- 1.3B-pruned	Sheared-Llama- 1.3B	Sheared-Llama- 1.3B-sharegpt	Sheared-Llama- 2.7B-pruned	Sheared-Llama- 2.7B	Sheared-Llama- 2.7B-sharegpt
PCS	0.0000	0.0000	0.0000	0.0000	0.0000	0.0000
ICS	0.4927	0.3512	0.3510	0.6055	0.4580	0.4548
REEF	0.9368	0.9676	0.9710	0.9278	0.9701	0.9991
SELF	0.9810	0.9896	0.9897	0.9853	0.9914	0.9948

-pruned: the version without continued pre-training;
-sharegpt: the version with instruction tuning.

Table 6: Comparison of fingerprint similarity score on Llama2-7B unstructured pruned models

	Unstructured Pruning		
	Sparse-Llama-2-7B	Wanda-Llama-2-7B	GBLM-Llama-2-7B
PCS	0.9560	0.9620	0.9616
ICS	0.9468	0.9468	0.9478
REEF	0.9985	0.9986	0.9991
SELF	0.9950	0.9953	0.9954

Comparison of merged models detectability In the model merging scenario, a suspect model is often derived from multiple victim models via different techniques. Table 7 presents the fingerprint similarity scores between weight-merged model (EvoLLM-jp-7B), distribution-merged model (FuseLLM-7B), and their corresponding victim target models. The results demonstrate that SELF reliably detects weight merged models as related. For distribution merging case, however, SELF successfully identifies the relatedness between FuseLLM-7B and its base model (Llama-2-7B), but fails to link it to OpenLlama2-7B and MPT-7B. We analyze this limitation in the following paragraphs and highlight REEF’s weakness, despite its higher similarity score in Table 7.

High Risk of False Positives in REEF Although REEF achieves similarity scores above 0.62 for the related models (OpenLlama2-7B and MPT-7B) in Table 7, it exhibits a high risk of misclassifying unrelated models as related. To

Table 7: Comparison of fingerprint similarity score on merged models

Target models	Weight Merging (EvoLLM-jp-7B)			Distribution Merging (FuseLLM-7B)		
	Shisa-gamma-7B-v1	Wizard-math-7B-1.1	Abel-7B-002	Llama-2-7B	OpenLlama2-7B	MPT-7B
PCS	0.9992	0.9990	0.9989	0.9997	0.0194	0.0000
ICS	0.9992	0.9988	0.9988	0.1043	0.2478	0.1014
REEF	0.9635	0.9526	0.9374	0.9996	0.6713*	0.6200*
SELF	0.9693	0.9911	0.9962	0.9949	0.0174	0.0051

* indicates a potential judgment as unrelated.

demonstrate this, we construct a focused comparison using Llama2-7B and seven distinct unrelated models (Table 8). Following the settings in [8], we evaluate REEF using representation-based fingerprinting (CKA on the 18_{th} layer) across 200 samples from five datasets: TruthfulQA ([33]), ConfAIde ([34]), PKU-SafeRLHF ([35]), ToxiGen ([36]), and SST2 ([37]).

As shown in Table 8, REEF’s similarity scores for unrelated models are inconsistently high, exceeding **0.67** on the SST2 dataset. This suggests that a threshold set to detect OpenLlama2-7B (0.6713) would incorrectly flag unrelated models as infringed. In contrast, our SELF method maintains consistently low scores (<0.3) for unrelated models, demonstrating superior robustness against false claim attacks.

Table 8: Comparison of Llama2-7B unrelated models fingerprint similarity output

Method	Dataset	Mistral-7B	MPT-7B	InternLM2.5	GPT2-Large	Cerebras-GPT	Pythia-6.7B	OPT-6.7B
REEF	TruthfulQA	0.1975	0.2111	0.1942	0.2320	0.2257	0.2307	0.2437
	ConfAIde	0.2340	0.2449	0.2308	0.2464	0.2471	0.2723	0.2419
	PKU-SafeRLHF	0.5099	0.5150	0.4307	0.4808	0.4390	0.4844	0.4764
	ToxiGen	0.5894	0.5528	0.6067	0.5366	0.6358	0.6151	0.4716
	SST2	0.6772	0.6221	0.6628	0.6034	0.5945	0.6783	0.5982
SELF		0.0050	0.0050	0.0050	0.2372	0.2874	0.0002	0.0009

Furthermore, REEF’s performance on *true* victim models is also sensitive to the dataset used. Table 9 shows the similarity output of REEF when verifying the actual source models of FuseLLM-7B on the problematic datasets (PKU-SafeRLHF, ToxiGen and SST2) identified above. For example, on ToxiGen, the score for the true victim model OpenLlama2-7B drops to **0.5614**, which is indistinguishable from the scores of unrelated models (e.g., Mistral-7B at 0.5894 in Table 8). This overlap confirms that REEF lacks a clear decision boundary to distinguish distribution-merged models from unrelated ones, whereas SELF demonstrates consistent discriminative capability across all test scenarios.

Table 9: Similarity output of REEF on FuseLLM-7B’s source models across different datasets

Model	PKU-SafeRLHF	ToxiGen	SST2
OpenLlama2-7B	0.5265	0.5614	0.6356
MPT-7B	0.5140	0.6360	0.7317

Our hypothesize We hypothesize that the challenges faced by all methods in detecting FuseLLM-7B’s relation to OpenLlama2-7B and MPT-7B stems from the unique fusion mechanism of distribution merging. The distribution merged model does not directly steal its victim models’ weights; instead, it is trained using the output distribution of the victim models. In the case of FuseLLM-7B, Llama-2-7B is adopted as the base model while OpenLlama2-7B and MPT-7B only provide output distribution for training. Consequently, methods based on model weight analysis may still detect merged model’s relatedness to its base model but are extremely difficult to detect such output distribution-based infringement. To address such limitation, we propose that future detection frameworks adopt a hybrid approach, combining weight-based metrics for base model identification with output-consistency checks for distilled knowledge. This dual strategy would ensure robust detection coverage across both architectural reuse and distribution-based fusion scenarios.

D Exploring Fingerprint Distance For Discrimination

This section evaluates SELF’s effectiveness across routine models using fingerprint distance. Routine models are defined as publicly available models with known relationships (related or unrelated) to the target model, as listed in

Table 1 of Section 5.1. The L2 distance between the fingerprints extracted from the target model and its related models (fine-tuned, pruned, quantized, or distilled variants) and unrelated models is computed. A smaller fingerprint distance indicates a higher likelihood that the two models are related.

Table 10 reports the distance between fingerprints extracted from the target models (Qwen2.5-7B and Llama2-7B) and their respective suspect models (both related and unrelated). For both target models, their distance exhibit a clear separation between related and unrelated cases (>0.95 for unrelated models and <0.65 for related models), with a sufficient margin (0.3) validating the discriminative power of our fingerprinting method. While our approach reliably detects IP infringement using fingerprint distance, the margin between the two categories is notably smaller than the margin (>0.7) achieve with *SimNet*, further underscoring the importance and necessity of *SimNet*. Additional evaluation and discussion can be found in Section E.5.

Table 10: Fingerprint Distance (Target Models: Qwen2.5-7B and Llama2-7B)

Qwen2.5-7B Unrelated		Qwen2.5-7B Related		Llama2-7B Unrelated		Llama2-7B Related	
Model	Distance	Model	Distance	Model	Distance	Model	Distance
Mistral-7B-V0.3	1.3050	Fine-tuned Variants		Mistral-7B-V0.3	0.9675	Fine-tuned Variants	
Llama2-7B	1.5112	Qwen2.5-7B-Instruct	0.0298	Qwen1.5-7B	1.2017	Llama2-7B-Chat	0.0408
Baichuan2-7B	2.0768	Qwen2.5-Math-7B	0.4692	Baichuan2-7B	1.5762	CodeQwen2.5-7B	0.6358
InternLM2.5-7B	1.5717	Qwen2.5-Coder-7B	0.4946	InternLM2.5-7B	1.6968	Llemma-7B	0.5739
GPT2-Large	1.6143	TableGPT2-7B	0.0528	GPT2-Large	1.4820	Pruned Variants	
Cerebras-GPT-1.3B	2.0006	Qwen2.5-7B-Medicine	0.0328	Cerebras-GPT-1.3B	1.6188	Sheared-Llama-2.7B	0.4376
ChatGLM2-6B	1.9483	Qwen2.5-7B-abliterated-v2	0.0307	ChatGLM2-6B	1.6980	SparseLlama-2-7B	0.1961
OPT-6.7B	2.9490	Quantized Variants		OPT-6.7B	2.6365	Quantized Variants	
Pythia-6.9B	1.5799	Qwen2.5-7B-4bit	0.0002	Pythia-6.9B	2.3580	Llama2-7B-4bit	0.0005
MPT-7B	2.1532	Qwen2.5-7B-8bit	0.0002	MPT-7B	1.6858	Llama2-7B-8bit	0.0005

Table 11 reports the pairwise fingerprint distances between the ten unrelated models listed in Table 10. It can be observed that the distances between the fingerprints of these unrelated models are all >1 . This confirms that our method can accurately distinguish unrelated models and thus avoid false positives.

Table 11: Fingerprint Distance between Unrelated Models

	Mis	Qwe	Bai	Int	Gpt	Cer	Cha	OPT	Pyt	MPT
Mistral-7B-V0.3		1.0114	1.8145	1.5130	1.7239	1.8124	1.5797	2.8946	2.2746	1.9419
Qwen1.5-7B	1.0114		1.5932	1.5750	1.5081	1.8140	1.9056	2.6926	1.9453	1.8204
Baichuan2-7B	1.8145	1.5932		2.5250	1.8923	1.9126	2.2444	2.5207	2.8323	1.8068
InternLM2.5-7B	1.5130	1.5750	2.5250		2.4088	2.6447	2.4530	3.5071	1.5415	2.4680
GPT2-Large	1.7239	1.5081	1.8923	2.4088		1.2487	1.8379	2.0373	2.6276	1.7582
Cerebras-GPT-1.3B	1.8124	1.8140	1.9126	2.6447	1.2487		1.8842	1.9259	2.9951	1.9990
ChatGLM2-6B	1.5797	1.9056	2.2444	2.4530	1.8379	1.8842		2.7989	3.1283	2.1770
OPT-6.7B	2.8946	2.6926	2.5207	3.5071	2.0373	1.9259	2.7989		3.7288	2.4523
Pythia-6.9B	2.2746	1.9453	2.8323	1.5415	2.6276	2.9951	3.1283	3.7288		2.8906
MPT-7B	1.9419	1.8204	1.8068	2.4680	1.7582	1.9990	2.1770	2.4523	2.8906	

To validate the effectiveness of our method on distilled models, we evaluated three DeepSeek distillation models of varying sizes and architectures. As shown in Table 12, their distance from respective base models remain < 0.3 , confirming their relatedness.

Table 12: Fingerprint Distance of DeepSeek models

Base Model	Distilled Model	Distance
Qwen2.5-Math-1.5B	DeepSeek-R1-Distill-Qwen-1.5B	0.1756
Qwen2.5-Math-7B	DeepSeek-R1-Distill-Qwen-7B	0.1266
Llama-3.1-8B	DeepSeek-R1-Distill-Llama-8B	0.2748

E Details of *SimNet*

This section presents the implementation details of *SimNet*, including its network architecture and training settings, as well as its impact on SELF’s robustness. The input of the SimNet is the suspect model’s fingerprint F_S , and the output is the similarity score range in $[0, 1]$.

E.1 Architecture

The overall architecture of the *SimNet* is shown in Table 13.

Table 13: Neural Network Architecture of SimilarityNet (Input Shape: $(B, 4N_{\mathcal{F}}, h)$)

Component	Type	Input Shape	Output Shape
Input	-	$(B, 4N_{\mathcal{F}}, h)$	-
unsqueeze	Dimension Expansion	$(B, 4N_{\mathcal{F}}, h)$	$(B, 1, 4N_{\mathcal{F}}, h)$
conv1 + bn1 + ReLU	Conv2d, BatchNorm2d, Activation	$(B, 1, 4N_{\mathcal{F}}, h)$	$(B, 64, 4N_{\mathcal{F}}, h)$
layer1	ResidualBlock $\times 2$, Stride 1	$(B, 64, 4N_{\mathcal{F}}, h)$	$(B, 64, 4N_{\mathcal{F}}, h)$
layer2	ResidualBlock $\times 2$, Stride 2	$(B, 64, 4N_{\mathcal{F}}, h)$	$(B, 128, 2N_{\mathcal{F}}, h/2)$
layer3	ResidualBlock $\times 2$, Stride 2	$(B, 128, 2N_{\mathcal{F}}, h/2)$	$(B, 256, N_{\mathcal{F}}, h/4)$
layer4	ResidualBlock $\times 2$, Stride 2	$(B, 256, N_{\mathcal{F}}, h/4)$	$(B, 512, N_{\mathcal{F}}/2, h/8)$
layer5	ResidualBlock $\times 2$, Stride 1	$(B, 512, N_{\mathcal{F}}/2, h/8)$	$(B, 512, N_{\mathcal{F}}/2, h/8)$
avgpool	AdaptiveAvgPool2d (1, 1)	$(B, 512, N_{\mathcal{F}}/2, h/8)$	$(B, 512, 1, 1)$
flatten (view)	View	$(B, 512, 1, 1)$	$(B, 512)$
fc	Linear	$(B, 512)$	$(B, 1)$
sigmoid	Activation	$(B, 1)$	$(B, 1)$
squeeze	Dimension Squeeze	$(B, 1)$	$(B,)$

In our experiments, $N_{\mathcal{F}}=8$, $h=256$.

E.2 Datasets

The *SimNet* training datasets for each target model includes the following models' fingerprints:

For Qwen2.5-7B: Qwen2.5-7B and its augmented model (label 1), Qwen2.5-7B-Instruct and its augmented model (label 1), MPT-7B and its augmented model (label 0), GPT2-Large and its augmented model (label 0), and Mistral-7B-v0.3 and its augmented model (label 0).

For Llama2-7B: Llama2-7B and its augmented model (label 1), Llama2-7B-chat (label 1) and its augmented model, MPT-7B and its augmented model (label 0), InternLM2.5-7B and its augmented model (label 0), and Mistral-7B-v0.3 and its augmented model (label 0).

For Shisa-gamma-7B-v1: Shisa-gamma-7B-v1 and its augmented model (label 1), MPT-7B and its augmented model (label 0), InternLM2.5-7B and its augmented model (label 0), Llama2-7B and its augmented model (label 0).

For Wizard-math-7B-1.1: Wizard-math-7B-1.1 and its augmented model (label 1), MPT-7B and its augmented model (label 0), InternLM2.5-7B and its augmented model (label 0), Llama2-7B and its augmented model (label 0).

For Abel-7B-002: Abel-7B-002 and its augmented model (label 1), MPT-7B and its augmented model (label 0), InternLM2.5-7B and its augmented model (label 0), Llama2-7B and its augmented model (label 0).

For OpenLlama2-7B: OpenLlama2-7B and its augmented model (label 1), MPT-7B and its augmented model (label 0), InternLM2.5-7B and its augmented model (label 0), Llama2-7B and its augmented model (label 0).

For MPT-7B: MPT-7B and its augmented model (label 1), Mistral-7B-v0.3 and its augmented model (label 0), InternLM2.5-7B and its augmented model (label 0), Llama2-7B and its augmented model (label 0).

E.3 Hyperparameter

The model was trained using the AdamW optimizer with an initial learning rate of 1×10^{-4} and weight decay of 1×10^{-6} , combined with a step learning rate scheduler (step size = 100, $\gamma = 0.8$). We minimized the binary cross-entropy loss with label smoothing ($\eta = 0.01$) and incorporated adversarial training through gradient sign perturbations ($\epsilon = 1 \times 10^{-5}$). Training proceeded for 1000 epochs, using PyTorch's default parameter initialization scheme and random seed 42.

For each augmentation type, we generate three augmented models with the following parameters:

- Gaussian Noise: The strength α is 0.1, 1, 10.
- Row Deletion: The number of deleted rows n_r is 10, 100, 1000.
- Column Deletion: The number of deleted columns n_c is 10, 100, 1000.
- Random Masking: The mask rate r is 0.1, 0.25, 0.5.

E.4 Overhead

SimNet requires only one-time training per target model and can be reused for all subsequent detections, ensuring that the computational overhead is amortized over time. Training *SimNet* takes about 2.5 minutes using a single RTX4090 GPU, while one inference takes less than 0.1 seconds. Despite this minimal overhead, our experiments demonstrated that *SimNet* delivers superior performance compared to existing methods, striking an optimal cost-benefit balance for practical deployment.

E.5 Impact of *SimNet* on Robustness

This section evaluates the impact of employing *SimNet* on method robustness. Using Llama2-7B as the target model, we evaluate both the distance and the similarity score in detecting related models obtained via the commonly used fine-tuning and pruning attacks.

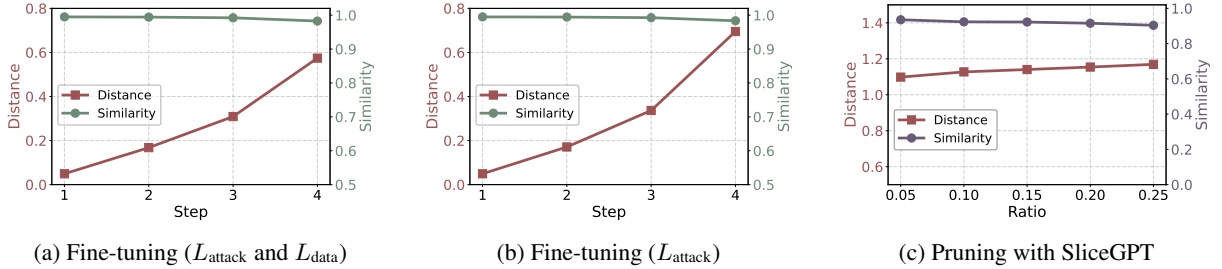


Figure 6: Fingerprint similarity and distance change of Llama2-7B under different attacks. (a) and (b) show the results under fine-tuning attacks. (c) shows the results under SliceGPT pruning.

***SimNet* enhances SELF’s robustness** As shown in Figure 6a and 6b, as fine-tuning steps increase, the distance (ideal: small for related models) between Llama2-7B (target model) and its variant grows quickly, while the similarity (ideal: high for related models) score remains consistently stable high – highlighting *SimNet*’s superior robustness in detecting fine-tuned models. For pruning attacks (Figure 6c), *SimNet* maintains high similarity scores (>0.9) even when the distance falsely indicted unrelated models (>1). This further confirms that *SimNet* can capture intrinsic features beyond distance, thereby ensuring the robustness of SELF against adversarial modifications.

F Ablation Study on Fingerprint Extraction

Table 14: Fingerprint Margin in Different Weight Component Settings

Invariant	Layer Selection			Weight Selection		
	First 8 Layers	Middle 8 Layers	Last 8 Layers	W_Q, W_K	W_V, W_O	Both
Singular Value	0.1484	-0.1366	-0.2020	0.1744	-0.0744	0.1484
Eigenvalue	0.2362	-0.0789	-0.2475	0.2283	-0.1538	0.2362
Both	0.3319	-0.1380	-0.1263	0.3382	-0.0217	0.3319

Table 15: Fingerprint Margin under Different h and $N_{\mathcal{F}}$ Settings

Invariant	Varying h				Varying $N_{\mathcal{F}}$			
	32	64	128	256	2	4	6	8
Singular Value	0.0486	0.0731	0.1478	0.1484	-0.0878	0.0816	0.1443	0.1484
Eigenvalue	-0.0306	0.0339	0.1345	0.2362	0.0921	0.1375	0.1467	0.2363
Both	0.0653	0.1732	0.2624	0.3319	0.0911	0.2080	0.2794	0.3319

In this section, we assess how different settings affect fingerprint extraction. We define the **fingerprint margin** as the difference between: 1) the minimum L2 distance among unrelated models’ fingerprints, and 2) the maximum L2 distance among related models’ fingerprints. Here, we have considered all models appeared in Tables 10 to 12. A large

positive margin indicates clearer distinguishability between related and unrelated models, while a negative margin suggests that some unrelated models exhibit smaller fingerprint distance than the maximum observed among related models. Accordingly, we systematically investigate the impact of the following settings on the fingerprint margin:

1. Invariant matrix construction choice (singular values or eigenvalues)
2. Transformer block layers selection (e.g. early vs. late layers)
3. Weight selection (e.g. W_Q and W_K vs. W_V and W_O)
4. Parameter h (top- h singular values / eigenvalues are selected to form the fingerprint)
5. Parameter $N_{\mathcal{F}}$ (how many layers are selected to form the fingerprint)

As shown in Table 14, the first eight layers offer larger fingerprint margins, indicating stronger differentiation between related and unrelated models than other layers. Although using only W_Q and W_K can achieve nearly comparable margin, to ensure that the fingerprint contains more information and thereby guarantees the performance of *SimNet*, we also include W_V and W_O as a source for fingerprint extraction.

Table 15 confirms that even small h and $N_{\mathcal{F}}$ can provide discriminative capability, while larger h and $N_{\mathcal{F}}$ leads to a greater fingerprint margin. The selection of h should ensure robust fingerprint extraction while being practical for deployment across diverse model sizes, i.e., smaller than any model’s d and d_{model} . Thus, we chose $h = 256$ and $N_{\mathcal{F}} = 8$ in our experiments, which is compatible with most LLMs’ weight dimensions.